Engineering and Applied Science Letters

PSR Press

Article

Optimization of nano-lead chromate additives as mechanical tensile promoters for cementitious composites

Naglaa F. Oriby[1], Labiba A. Marzouk[2] and Khaled M. Elsabawy[1,*]

[1] Chemistry Department, Materials Unit, Faculty of Science, Tanta University, Tanta - 31725, Egypt
[2] Higher Institute of Engineering and Technology, Tanta-Egypt
* Correspondence: khaledelsabawy@yahoo.com

Received: 28 January 2026; Accepted: 10 March 2026; Published: 30 March 2026.

Abstract: This study presents the synthesis, application, and dosage optimization of nano-lead chromate as a microstructural modifier for cementitious composites. $PbCrO_4$ nanoparticles were incorporated into cement-paste specimens at addition levels of 5, 10, 20, 40, 80, and 100%, defined with respect to the stoichiometric SiO_2 content of the cement and also reported for comparison with conventional binder-based formulations. The resulting composites were evaluated by X-ray diffraction, FTIR, UV/Vis., TGA/DTA, SEM, EDX, and TEM in order to relate phase development and microstructural features to mechanical performance. Mechanical response was assessed from replicated loading tests at 7 and 28 days, and the recorded failure loads were used to estimate indirect tensile behavior for the prismatic specimens. The results indicate that nano-$PbCrO_4$ modifies the texture and compactness of the cementitious matrix and increases the measured load-bearing capacity within the investigated dosage range. The study therefore provides an exploratory assessment of $PbCrO_4$ as a nano-scale mechanical promoter, while practical implementation would require additional durability and environmental verification.

Keywords: lead chromate, cementitious composite, IR, mechanical tensile, XRD, TEM

1. Introduction

It is well established that Portland cement is the principal binder used in modern construction. Nevertheless, plain cementitious matrices remain brittle and exhibit limited strain capacity and weak tensile resistance, which restrict their crack tolerance and long-term durability under service loading.

The tensile response of reinforced concrete can be improved by adding crack-controlling elements such as steel bars, fibers, and other promoters that delay the initiation and propagation of microcracks [1,2].

In recent years, nano-scale additives such as graphene, carbon nanotubes, and nano-silica have attracted considerable interest as reinforcing agents for cement-based materials because they can interact with defects at a much smaller scale than conventional reinforcement [3]. Nano-silica, for example, has been shown to improve the mechanical response of cement matrices [4].

Nano-silica has a specific surface area of about 300 m^2/g and a predominantly spherical morphology with particle diameters below 30 nm [5]. Its beneficial action is commonly attributed to two mechanisms [6]: first, a nucleation effect that promotes cement hydration because of the high specific surface area, and second, a filler effect that densifies the microstructure by occupying spaces comparable to gel pores. At the same time, its low aspect ratio limits its ability to restrain crack growth once localized defects begin to propagate.

Accordingly, there remains a need to examine alternative nano-additives that may modify matrix texture, interfacial bonding, and resistance to crack development. In parallel, the broader field has shown that non-metallic and textile-type reinforcement systems can markedly improve the mechanical behavior of cementitious materials under different loading conditions [7–15].

Elsabawy et al. [16–18] previously reported that soft-metal additions can enhance the ductility and flexibility of selected ceramic and superconducting systems. Motivated by that concept, the present work explores whether nano-scale $PbCrO_4$ can play a related microstructural role in a cementitious matrix.

The objective of this study is therefore to evaluate nano-lead chromate as a cement-compatible additive and to identify the dosage range that provides the most favorable combination of phase characteristics,

microstructural compactness, and measured mechanical response in cement-paste composites. The work is intended as an exploratory materials study focused on synthesis, characterization, and short-term mechanical performance within the investigated laboratory conditions.

2. Experimental

2.1. Synthesis and characterization of nano-$PbCrO_4$ promoter

Lead chromate nanoparticles were synthesized by chemical co-precipitation. Lead nitrate (20 g) and potassium chromate (40 g) were dissolved separately in 150 mL of distilled water and then combined slowly under continuous stirring. The resulting precipitate was allowed to settle, separated by suction filtration, washed repeatedly with distilled water and ethanol, dried, and finally ground in an agate mortar [19]. The synthesized powder was characterized by powder X-ray diffraction, scanning electron microscopy, ultraviolet spectroscopy, Fourier transform infrared spectroscopy, and TEM. These measurements confirmed the formation of crystalline lead chromate nanoparticles with particle sizes in the approximate range of 47–93 nm and with a well-developed particulate morphology. FTIR analysis was further used to identify the main vibrational features of the synthesized material before its incorporation into the cementitious matrix.

2.2. Methods and applied instruments

PXRD patterns were collected at room temperature using CuKα radiation on a MiniFlex II powder X-ray diffractometer (Rigaku, Japan). The scanning range was 2θ = 5–55°, the operating voltage was 30 kV, the current was 15 mA, and the scanning rate was 4°/min. UV/Vis. spectra were measured using a Shimadzu double-beam spectrophotometer with the nujol mull technique.

Thermal behavior was examined by TGA/DTA using a Perkin Elmer Pyris STA 6000 thermogravimetric analyzer. Approximately 0.2 g of green cement powder was placed in the sample pan with alumina as the reference, and the temperature was increased from room temperature at a rate of 1^{o}C/min. Scanning electron microscopy (SEM), transmission electron microscopy (TEM), and EDX elemental analysis were used to evaluate morphology and elemental distribution. FTIR spectra were recorded on a Shimadzu FT-IR-8101A spectrophotometer in the 4000–400 cm^{-1} range.

2.3. Synthesis of cement-paste composites samples

2.3.1. Cementitious materials

The materials used in the experimental program are described below. The mortar mixes were prepared from ordinary Portland cement, fine aggregate, water, the nano-$PbCrO_4$ promoter, and a superplasticizer. Natural siliceous sand was used as the fine aggregate throughout the study [20].

2.3.2. Sieve analysis of fine aggregates according to egyptian code 203/2017

The sand was clean and free from visible impurities, with a specific gravity of 2.65, a fineness modulus of 2.55, and an absorption ratio of 0.81%. It was sieved to obtain standard grading in accordance with Egyptian code 203/2017 for preparation of the mortar test specimens. The sieve analysis results are presented in Table 1 and Figure 1.

Table 1. Results of sieve analysis for fine aggregates

Sieve size mm	9.51	4.75	2.36	1.18	0.6	0.3	0.15
%passing	100	90-100	80-100	50-85	25-60	10-30	2-10
%passing sand used	0	3	3	81	53	18	2

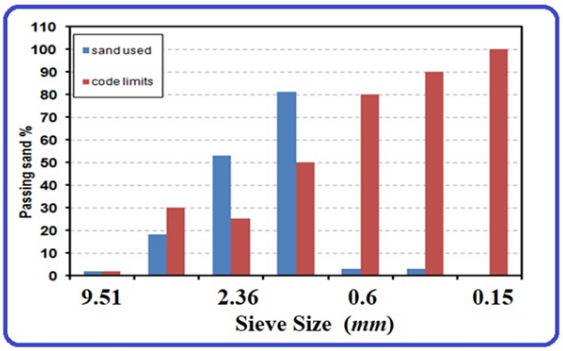

Figure 1. Sieve analysis results for fine aggregates

2.3.3. Applied Cement Descriptions

A local ordinary Portland Suez cement (OPC CEM I 42.5 N) was used as the matrix binder. The cement exhibited initial and final setting times of about 2 and 5 h, respectively. All cement characterization tests were conducted in accordance with the relevant standard specifications for Portland cement [20,21]. The chemical composition of the cement is listed in Table 2.

Table 2. Chemical composition of ordinary Portland cement manufacture specifications

Constituents	Concentration in Weight (%)
Silica as Si O_2	19.8
Alumina as AL_2 O_3	5.6
Iron as Fe_2 O_3	2.4
Potassium as k_2 O	0.58
Calcium as Ca O	65.9
Sodium as Na_2 O	0.29
Sulphur as SO_3	2.8
Loss in ignition	1.2
Insoluble residue	0.4
Free lime	0.9
Lime Saturation Factor	100.4
Lime Combination Factor	98.9
Silica ratio	2.48
Alumina ratio	2.33
Tricalcium Cilicate (C_3 S)	65.1
Dicalcium Silicate (C_2S)	7.6
Tricalcium Aluminate (C_3A)	10.8
Tetracalcium Aluminate Ferrite (C_4 AF)	7.3

2.3.4. Chemical admixtures (super plasticizer)

A superplasticizer complying with ASTM C494 Type F and B.S. 5075 Part 3, with a specific gravity of 1.2, was used to provide the required workability for the mortar mixtures. The commercial product used was Addicrete BVF. The recommended dosage range is 0.5–2% by weight of cementitious material [20–22].

2.3.5. Mechanical properties of mixes

The mix design included ordinary Portland cement, sand, water, the promoter, and a superplasticizing agent. The objective was to determine the highest practical promoter dosage that could enhance the mechanical response of the mortar matrix without adversely affecting mixture preparation or specimen integrity. All mixes were prepared at a constant water/cement ratio of 0.35, while the superplasticizer dosage was fixed at 2% by weight of cement to maintain workable consistency. The dry constituents were first blended thoroughly, after which the mixing water was added and the batch was remixed manually to obtain a uniform paste. Seven mortar mixtures were investigated, comprising one control mixture and six promoter dosages from 5% to

100%. The mix proportions are listed in Table 3, and representative images of the tested mixtures are given in Figure 2. For each mixture, prismatic specimens with dimensions of 20 × 20 × 25 mm were cast for the loading tests.

Table 3. Mortar mix properties per batch

MIX	Cement (Kg)	Promoter (gm)	Percentage of promoter	Sand (Kg)	Water (Kg)	Super-Plasticizer (Kg)
M1	0.0426	0	0%	0.0085	0.002	0.00008
M2	0.0426	0.425	5%	0.0085	0.002	0.00008
M3	0.0426	0.85	10%	0.0085	0.002	0.00008
M4	0.0426	1.7	20%	0.0085	0.002	0.00008
M5	0.0426	3.4	40%	0.0085	0.002	0.00008
M6	0.0426	6.8	80%	0.0085	0.002	0.00008
M7	0.0426	8.5	100%	0.0085	0.002	0.00008

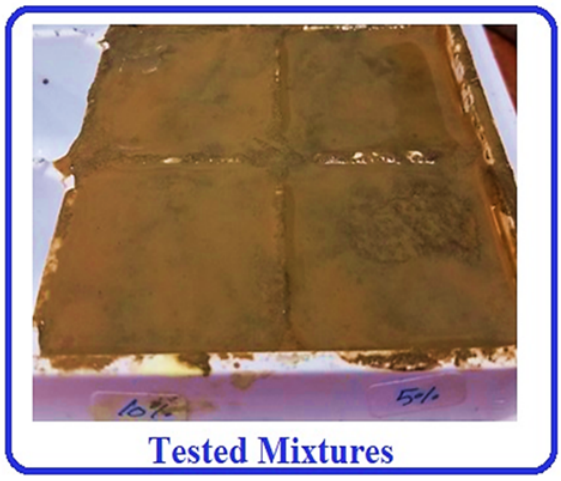

Figure 2. Images of the tested mixtures

A total of 42 specimens were prepared to improve the reliability of the mechanical dataset (7 mixes × 3 replicates per curing age × 2 testing ages). After casting, all specimens were demolded after 24 h and transferred to lime-saturated water for curing at 23 ± 2 °C and relative humidity above 95% until testing at 7 and 28 days.

2.3.6. Mechanical performance measurements

Mechanical tensile test set-up and instrumentation. The specimens were tested under monotonic compressive loading at 7 and 28 days using a hydraulic loading machine in accordance with standard laboratory practice [3,20,22]. The load was applied continuously at a constant rate of 0.5 N/mm^2 until failure. The testing machine is shown in Figure 3.

The ultimate load was read directly from the machine dial. In addition to the recorded first-crack and failure loads, these measurements were used to calculate the nominal compressive stress and to estimate the indirect tensile response discussed later for the tested prismatic specimens.

Figure 3. Loading machine used for the mechanical tests

3. Results and Discussions

3.1. Phase Identification of Cementitious Paste Composites

X-ray diffraction was used to identify the principal crystalline phases present in the hardened cementitious composites [23–25]. The main reflections observed at 2θ values of 26.2, 29.39, 32.5, 36, 39.47, 42.46, 50.5, 54.8, 59.97, 67.74, 73.45, and 75.6 (Figure 4) correspond to the dominant fingerprint peaks of the control and promoter-containing samples. The overall diffraction behavior is consistent with the phase assemblages reported by Mollah et al. [24,25].

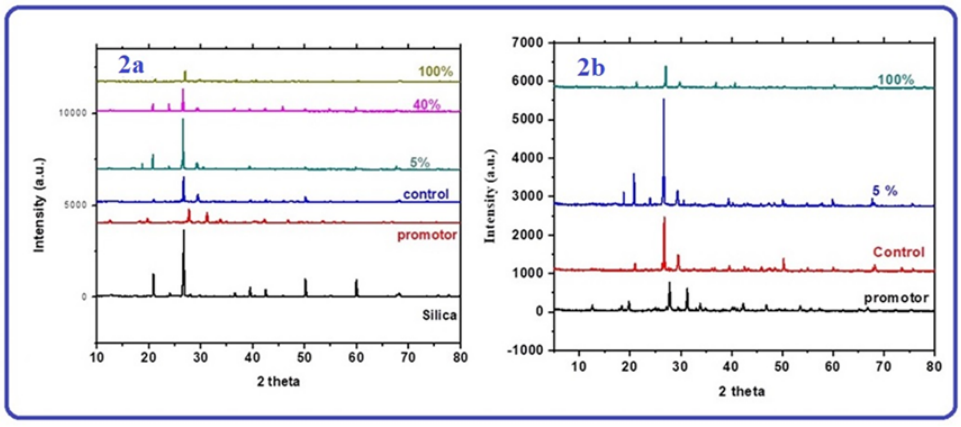

Figure 4. (a): X-ray patterns of promoter and the cementitious specimens with and without promoter. and (b): X-ray diffraction patterns for the promoter and cement blocks containing the minimum and maximum promoter ratios

In agreement with previous reports [23,24], the principal cement-related phases were identified as iron oxide (Fe_2O_3), belite (Ca_2SiO_4), and alite (Ca_3SiO_5). The diffractograms in Figure 4(a,b) also reflect the expected hydration products formed when alite and belite react with water, notably portlandite and amorphous calcium–silica–hydrate (C–S–H). Some $Ca(OH)_2$ reflections overlap with alite, belite, and ferrite peaks, which complicates strict phase separation in the hydrated matrix. In addition, calcium carbonate can form through secondary carbonation reactions involving portlandite and hydrated phases under ambient exposure [25]. The peaks assigned to chromate-containing phases appear at 2θ = 12.59, 18.32, 19.79, 27.77, 31.25, 33.83, 42.32, 46.85, 53.54, 55.64, 57.41, and 65.12, indicating the continued presence of the promoter-related crystalline component within the tested system.

3.2. Characterization of Cementitious Paste Composites

3.2.1. IR and UV/Vis. Spectral Measurements

A portion of each synthesized cement block was carefully ground and used for IR and UV/Vis. measurements. Potassium bromide (KBr) was used as the IR reference medium, whereas paraffin oil was used for the UV/Vis. measurements through the nujol mull technique, as shown in Figure 5(a-g) and Figure 5(h-l), respectively.

The principal IR absorption bands and their relative intensities are summarized in Table 4.

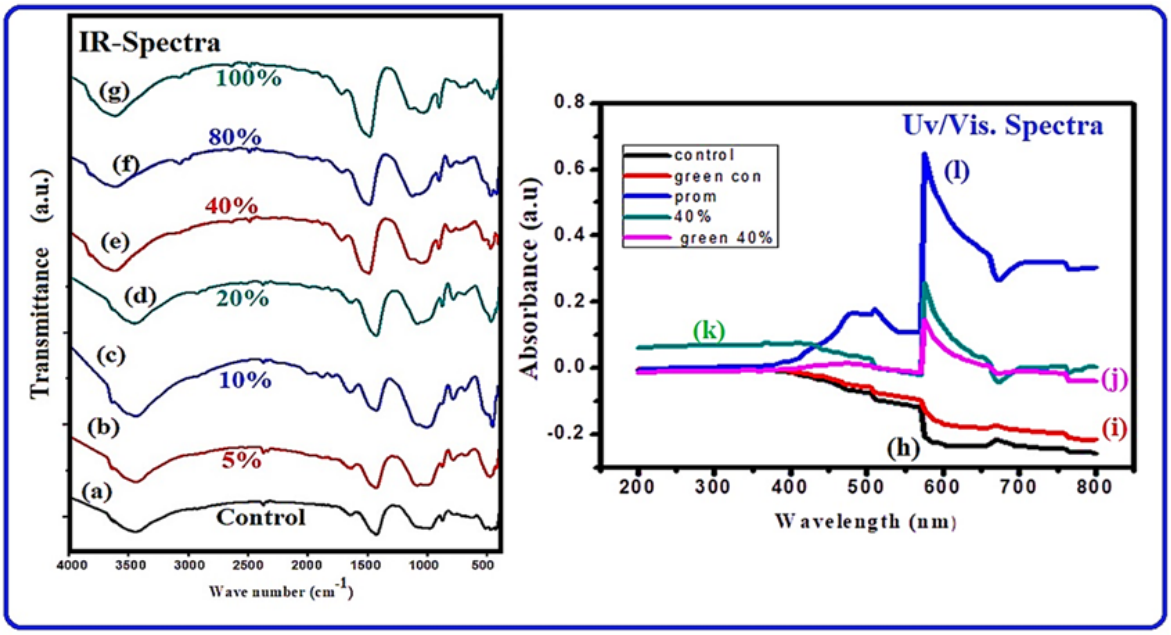

Figure 5. IR absorption and UV/Vis. spectra measured for cementitious samples from 0.0% to 100% promoter addition relative to the applied silicate basis

The principal vibrational bands identified in Figure 5(a-g) provide information on the silicate, sulphate, and carbonate groups that dominate the cementitious matrix [26].

The absorption band at 3641 cm^{-1} is attributed to free OH groups associated with Ca^{+2} (free lime) [27]. The broad band at 3441–3431 cm^{-1} is assigned to O–H stretching of physically adsorbed or bound water. The major silicate-related vibrations appear in the 1647–1631 cm^{-1} and 1431–1429 cm^{-1} regions, whereas the characteristic carbonate and sulphate bands are observed near 989–983 cm^{-1} and 875 cm^{-1}, respectively.

Figure 5(h-l) presents the UV/Vis. response of the control mortar, green control sample, 40% green sample, 40% mortar sample, and the promoter. The 40%-containing samples show a spectral profile closer to that of the promoter, including a pronounced absorption feature near 575 nm, whereas the promoter itself exhibits a broader hump around 485 nm. These observations support the interaction of the additive with the cementitious matrix and are broadly consistent with previous reports on modified cement systems [2,3,20].

Table 4. IR-absorption spectra for the cement blocks

Sample name	Band location in cm^{-1}						
	420-520	600-700	700-800	800-1100	1300-1650	1750-2000	2300-3000
promoter	-	-	-	819 (s,s) 893 (s,s)	1379 (s,m) 1630 (b,w)	1763(b,m)	2923 (b,w) 2371 (s,w)
silica	460(s,s)	689(s,w)	782(s,m)	1075(s,s)	1629(s.w)	1785(b,w) 1880(s,w)	2374(s,w)
control	474(s,s) 513(s,s)	617(b,m)	-	874(s,m) 983(b,s)	1430(s,s) 1647(s,m)	-	2372(s,w)
5%	472(s,s)	688(b,w)	788(s,w)	876(s,w) 1085(b,s)	1430(s,s) 1647(s,m)	-	2370(s,w)
10%	454(s,s)	686(s,w)	786(s,m)	1007(b,s)	1430(s,m) 1647(b,m)	1793(b,w) 1880(b,w)	2372(s,w)
20%	477(s,s)	687(b,w)	784(s,m)	876(s,m) 1083(b,s)	1430(s,s) 1631(s,m)	1793(b,w) 1880(b,w)	2372(s,w) 2927(b,w)
40%	466(s,m)	-	718(b,w)	876(s,m) 1010(b,s)	1431(s,s) 1647(b,m)	-	2373(s,w)
80%	424(s,s) 467(s,s)	686(b,w)	787(s,w)	875(s,m) 1085(s,s)	1430(s,s) 1647(b,w)	1880(b,w)	2373(s,w) 2926(s,m)
100%	461(s,m) 515(s,w)	-	706(b,w)	874(s,m) 1000(b,m)	1430(s,s) 1647(b,w)	1793(b,w)	2374(s,w) 2336(s,w) 2518(b,w)

3.3. Thermo-Gravimetric Analyses Measurements

Figure 6(a-h) shows the TGA and DTA curves obtained for the green samples containing 0, 5, 40, and 100% promoter.

The TGA curves in Figure 6(a-d) can be divided into three main mass-loss regions. The first, with a weight loss of about 0.25–0.36%, is attributed mainly to evaporation of free and physically adsorbed water [3,5,28]. The second major loss occurs around 145^{o}C and ranges from 1.42 to 2.14%, while the third varies between 1.58 and 2.80%. These events are associated with dehydration and decomposition processes involving hydrated products and carbonate-containing phases in the cement system [2,3].

The DTA curves in Figure 6(e-h) exhibit three principal endothermic features. The first occurs below 100^{o}C and is mainly related to moisture loss. Endothermic effects between about 100 and 200^{o}C are associated with dehydration of hydration products including C–S–H. A higher-temperature endothermic event near 700^{o}C is attributed to carbonation-related decomposition and $CaCO_3$ breakdown [2,29].

3.4. Nano-structural features of cementitious composites

3.4.1. Scanning electron microscopy and EDX-elemental analysis

SEM and TEM were used to investigate the nanostructural characteristics of the cementitious composites.

Concrete is a heterogeneous composite consisting of aggregate particles, hydrated cement paste, and an interfacial transition zone (ITZ), and the quality of this microstructure strongly influences the resulting mechanical behavior [29,30].

Figure 7(a-e) shows the SEM images captured for the control sample (a), nano lead chromate (b), and different nano admixed systems (c-e), respectively.

Inspection of the SEM images indicates that the promoter modifies the contact zone between the hydrated matrix and the aggregate fraction, leading to improved compactness and better apparent bonding, in line with the general behavior discussed in [30]. In particular, the 5% composite shows a dense and comparatively homogeneous texture, suggesting more uniform nanoparticle distribution and fewer visible microcracks than the control. At higher dosages, the micrographs indicate less uniform dispersion.

On this basis, the 5% mixture appears to provide the most balanced microstructural refinement, which is also supported qualitatively by the EDX elemental maps in Figure 7(f-h).

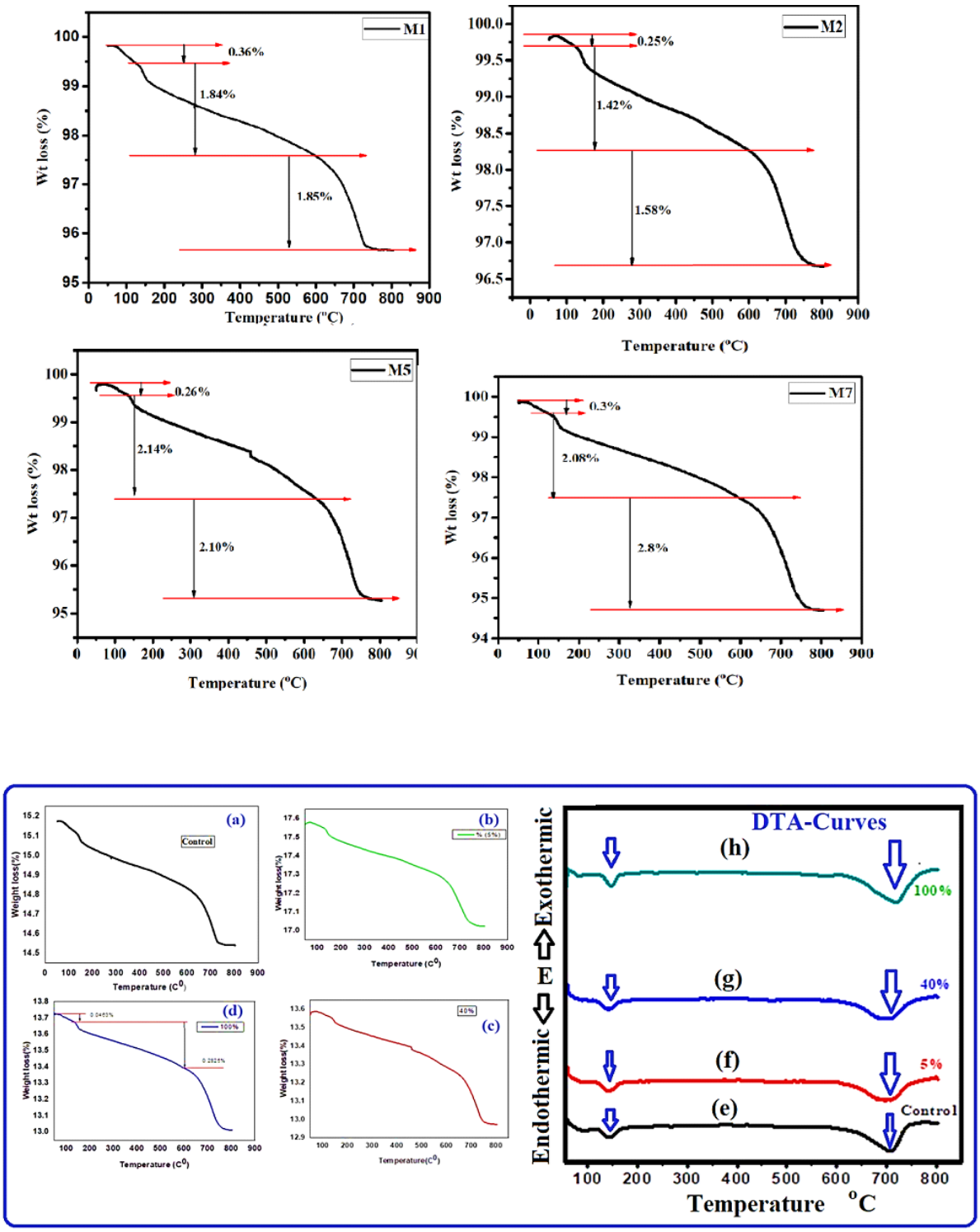

Figure 6. TGA and DTA curves measured for green cementitious mixtures containing 0.0, 5, 40, and 100% promoter, respectively

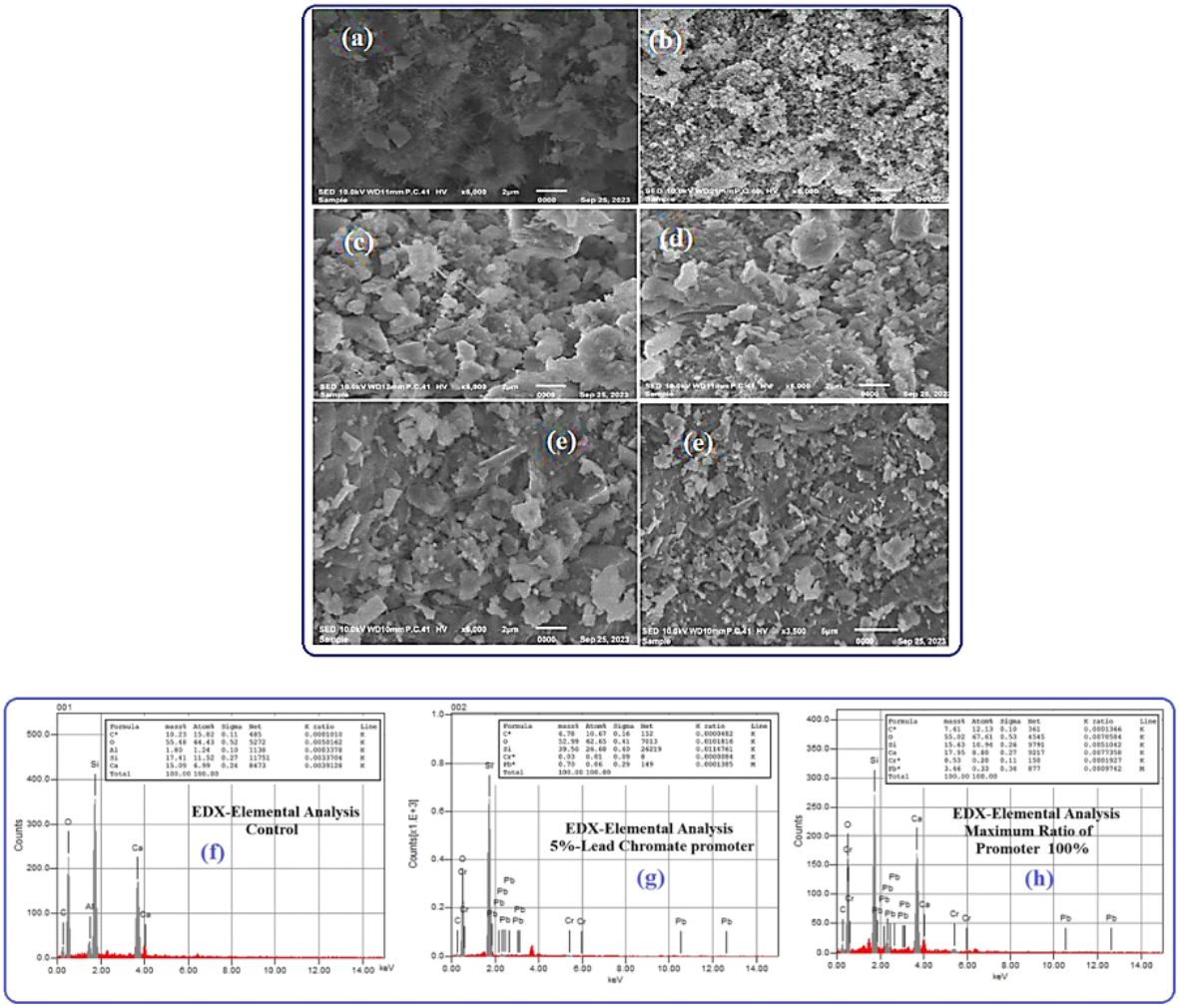

Figure 7. SEM images captured for: a) control cementitious sample, b) nano lead chromate, c) 5% cementitious composite, d) 40% composite and e) 100% composite sample with two different magnification factors 2 and 5 µm. While, f), g) and h) are EDX-elemental analysis for cementitious composites, namely, control sample (0.0% promoter), lower promoter ratio (5%), and higher promoter ratio of 100% respectively.

At the microscopic level, cement paste contains unreacted cement grains, pores, and hydration products such as calcium hydroxide, ettringite, and fibrous C–S–H [31]. The role of additives in high-performance cement systems is therefore to modify these phases and reduce the pore space through physical and chemical effects.

A reduction in capillary and gel porosity is generally associated with improved strength and durability [32]. The present observations suggest that the inclusion of lead chromate changes the local packing and texture of the matrix, producing a more compact morphology and fewer visible defects in comparison with the control. This interpretation is consistent with earlier work in which soft-metal additions were used to alter microstructural behavior in brittle materials [15,16].

In addition, previous studies have shown that the relative concentrations of lead and chromate ions can influence $PbCrO_4$ particle formation and growth [15,16,33]. In the present composites, the samples in Figure 7(c-e) appear more homogeneous than the control in Figure 7(a), indicating that the promoter contributes to a denser interfacial texture and improved bonding between the cement matrix and the dispersed phase [31].

3.4.2. Transmission electron microscopy (TEM)

The synthesized nanochromate powder as well as the applied silicate phase were characterized by TEM, and the corresponding images are shown in Figure 8(a-f).

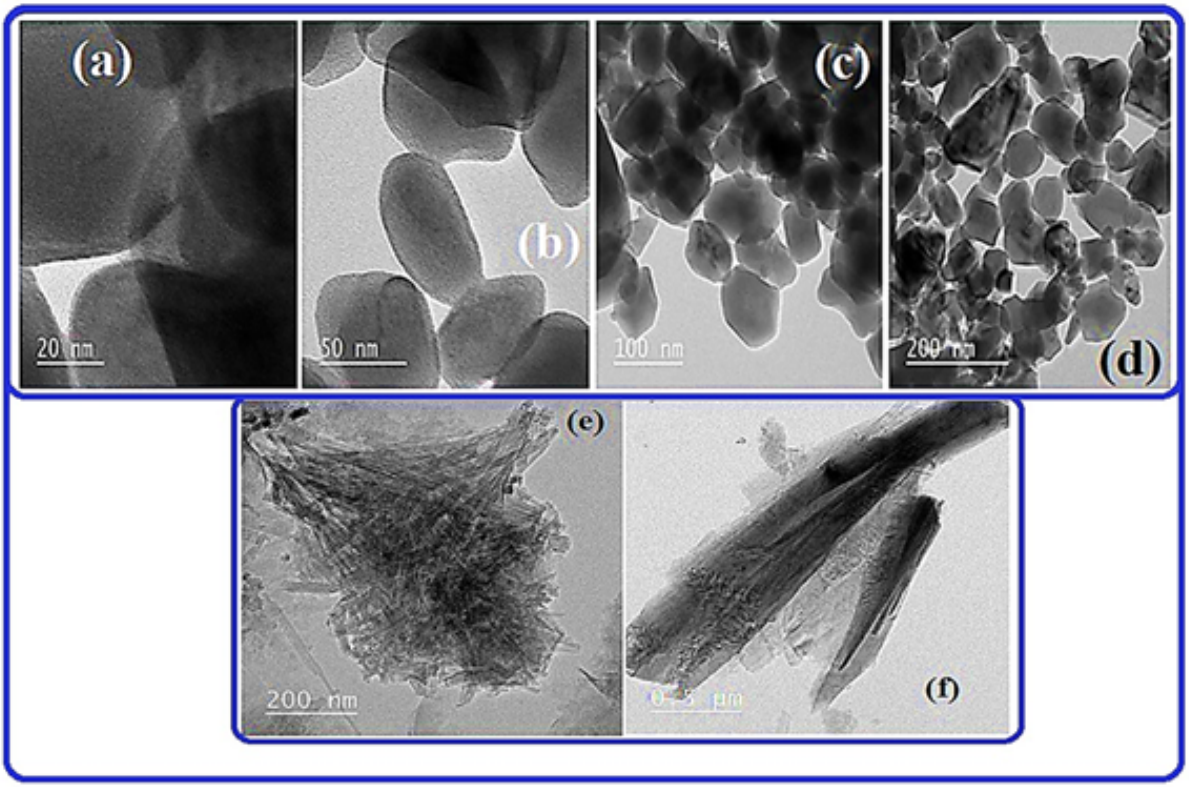

Figure 8. TEM images captured for applied nano-lead chromate with magnification factors ranging between (a) 20, (b) 50, (c) 100, and (d) 200 nm; (e) and (f) are TEM images of the applied silicates with magnification factors of 200 nm and 0.5 μm, respectively.

Analysis of the TEM images for the synthesized lead chromate confirms an average particle-size range of about 42–93 nm, as is especially clear in Figure 8(b,c). This nano-metric scale is favorable for dispersion within the cementitious matrix and supports the observed improvement in texture homogeneity and mechanical response [2,3,33]. The silicate images are also consistent with the morphologies reported previously for comparable cement-related materials [4,5,29].

3.5. Mechanical performance measurements

3.5.1. Compressive strength and ultimate load measurements

All specimens from mixtures M1 to M7 were tested using the loading machine shown in Figure 3, as described in the Experimental section. For each mixture, the first-crack load and the ultimate failure load were recorded, and the values plotted in Figure 9 correspond to the average of three independent destructive tests at each curing age.

Standard deviation bars are included in the plots to indicate the repeatability of the measurements. Within the investigated range, the load-bearing capacity increased progressively with promoter dosage. Figure 9 shows that the maximum ultimate load was 12.3 kN for M7, whereas the minimum value was 3.6 kN for the control mix M1 [15,16]. The maximum first-crack load was 2.3 kN for M7, while the minimum first-crack load was 0.2 kN for M1 and M2.

When these mechanical results are considered together with the SEM/EDX observations, the data suggest that the promoter contributed to improved matrix integrity and more effective stress transfer within the tested composites. The observed trend is also broadly consistent with earlier reports in which increasing soft-metal content was associated with enhanced mechanical response in brittle materials [16–18].

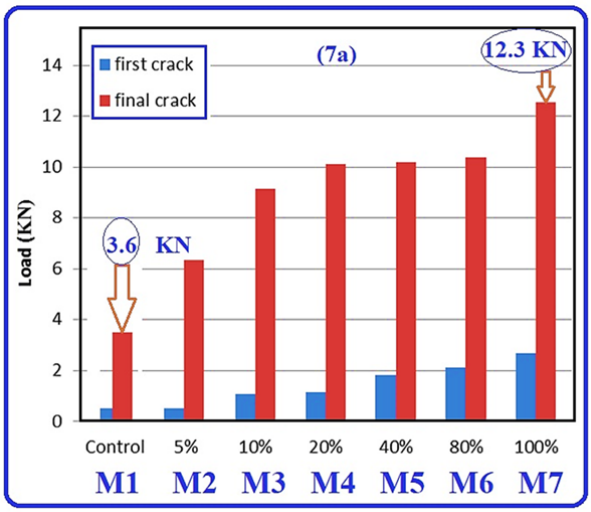

Figure 9. First-crack load and ultimate load for all synthesized cementitious composites

In the present evaluation, the first-crack load was taken as the onset of the initial deviation from linear response, whereas the ultimate load corresponds to the maximum load sustained before failure. The systematic increase in both quantities for the promoter-containing specimens indicates improved resistance to crack initiation and crack propagation under the applied loading conditions.

To obtain a tensile-related performance index from the measured failure loads, an empirical procedure [34,35] was used to estimate the indirect tensile stress for the prismatic cementitious specimens shown in Figure 9.

The indirect tensile stress (M_P) was estimated for the 20 × 20 × 25 mm specimens using

$M_P = 2kF/\pi DL$

where F is the failure load, L and D are the specimen dimensions, and k is a geometric correction factor introduced to account for the non-cylindrical specimen shape.

As shown in Figure 10, the estimated indirect tensile stress increased with promoter dosage from 5% to 100%. The maximum value, 1.42 MPa, was obtained for mixture M7, corresponding to an increase of about 355% relative to the control specimen. Within the limits of the present test program, this result indicates that the promoter improved the tensile-related performance of the mortar system.

This behavior is consistent with the microstructural observations and suggests that a more uniform $PbCrO_4$ distribution helps reduce local stress concentrations and delay microcrack development under load [16,17].

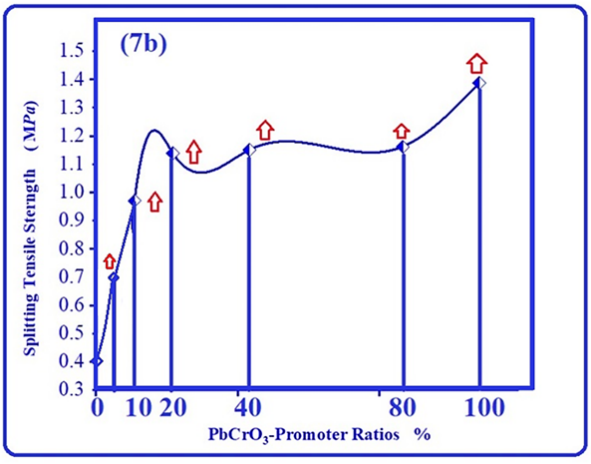

Figure 10. Estimated indirect tensile stress values adjusted for prismatic geometry

The magnitude of the observed improvement is promising when viewed against published results for other nano-additives. For example, Hamed et al. [36] reported that dispersing nano-clay at 5, 7.5, and 10% replacement levels improved the compressive, splitting tensile, flexural, and bond strengths by about 1.42 to 3.74 times compared with untreated nano-clay mixes. Likewise, Yehia [37] found that nano-clay additions of 3%, 5%, and 7% improved compressive, indirect tensile, and flexural strengths by 35%, 42%, and 41%, respectively. Although the materials and dosage definitions are not identical, these comparisons indicate that the present $PbCrO_4$ system yields a response that is competitive with other nano-modified cementitious composites.

4. Conclusions

The conclusive remarks of this study can be summarized as follows:

- The present investigation demonstrated the synthesis and application of nano-lead chromate as a microstructural and mechanical promoter for cementitious composites.
- The synthesized $PbCrO_4$ nanoparticles were successfully incorporated into the cementitious matrix and were identified by XRD, FTIR, UV/Vis., TGA/DTA, SEM, EDX, and TEM.
- The selected dosage range enabled comparison of the promoter effect over a wide interval of additions referenced to the cement silica content under the same curing and testing conditions.
- Microstructural observations indicated that promoter-containing specimens developed a denser and more homogeneous texture than the control, particularly at lower and intermediate dosages, which supports the measured improvement in load-bearing behavior.
- The tested composites exhibited a marked increase in estimated indirect tensile performance, reaching up to 3.55 times the control value for the highest dosage investigated.
- Within the limits of the present short-term laboratory study, nano-$PbCrO_4$ can therefore be considered a promising mechanical promoter; however, additional durability, leaching, and long-term performance studies are still required before practical application can be recommended.

Acknowledgments: The authors are thankful to the Partnership for Applied Sciences, Engineering, and Technology (PASET) - Regional Scholarship and Innovation Fund (RSIF) for the support of this study.

Conflicts of Interest: The authors certify that there is no conflict of interest whatsoever with any affiliation, or involvement with any organization, financial and non-financial entity.

References

[1] Chung, D. D. L. (2001). Comparison of submicron-diameter carbon filaments and conventional carbon fibers as fillers in composite materials. *Carbon, 39*(8), 1119–1125.

[2] Kosmatka, S. H., Kerkhoff, B., & Panarese, W. C. (2002). *Design and Control of Concrete Mixtures* (14th ed.). Portland Cement Association.

[3] Jo, B.-W., Kim, C., Tae, G., & Park, J.-B. (2007). Characteristics of cement mortar with nano-SiO_2 particles. *Construction and Building Materials, 21*(6), 1351–1355.

[4] Senff, L., Labrincha, J. A., Ferreira, V. M., Hotza, D., & Repette, W. L. (2009). Effect of nano-silica on rheology and fresh properties of cement pastes and mortars. *Construction and Building Materials, 23*(7), 2487–2491.

[5] Sanchez, F., & Sobolev, K. (2010). Nanotechnology in concrete–A review. *Construction and Building Materials, 24*(11), 2060–2071.

[6] Konsta-Gdoutos, M. S., Metaxa, Z. S., & Shah, S. P. (2010). Highly dispersed carbon nanotube reinforced cement-based materials. *Cement and Concrete Research, 40*(7), 1052–1059.

[7] Helbig, T., Unterer, K., Kulas, C., Rempel, S., & Hegger, J. (2016). Fuß- und Radwegbrücke aus Carbonbeton in Albstadt-Ebingen: Die weltweit erste ausschließlich carbonfaserbewehrte Betonbrücke. *Beton- und Stahlbetonbau, 111*, 676–685.

[8] Rempel, S., Kulas, C., Will, N., & Bielak, J. (2017). Extremely light and slender precast bridge made out of textile-reinforced concrete. In D. Hordijk & M. Luković (Eds.), *High tech concrete: Where technology and engineering meet* (pp. 2530–2537). Springer International Publishing.

[9] Rempel, S., Will, N., Hegger, J., & Beul, P. (2015). Filigrane Bauwerke aus Textilbeton: Leistungsfähigkeit und Anwendungspotenzial des innovativen Verbundwerkstoffs. *Beton- und Stahlbetonbau, 110*, 83–93.

[10] Hegger, J., Zell, M., & Horstmann, M. (2008). Textile reinforced concrete–Realization in applications. In *Proceedings of the International fib Symposium Tailor Made Concrete Structures: New Solutions for Our Society* (Amsterdam, The Netherlands, May 19–21, 2008).

[11] Curbach, M., & Ortlepp, R. (2012). *Sonderforschungsbereich 528: Textile Bewehrungen zur bautechnischen Verstärkung und Instandsetzung–Abschlussbericht: Gekürzte Fassung*. Sächsische Landesbibliothek–Staats- und Universitätsbibliothek Dresden.

[12] Hegger, J. (2012). *Sonderforschungsbereich 532: Textilbewehrter Beton–Grundlagen für die Entwicklung einer neuartigen Technologie*. Rheinisch-Westfälische Technische Hochschule Aachen.

[13] Jesse, F. (2004). *Tragverhalten von Filamentgarnen in zementgebundener Matrix* [Doctoral dissertation, Technische Universität Dresden].

[14] Herbrand, M., Adam, V., Classen, M., Kueres, D., & Hegger, J. (2017). Strengthening of existing bridge structures for shear and bending with carbon textile-reinforced mortar. *Materials, 10*, Article 1099.

[15] Bielak, J., Schöneberg, J., Classen, M., & Hegger, J. (2022). Shear capacity of continuous concrete slabs with CFRP reinforcement. *Construction and Building Materials, 320*, Article 126117.

[16] Elsabawy, K. M., Oraiby, N. F., & Fallatah, A. M. (2020). Narrow range of zinc oxide core–shell hollow microspheres dopings for mechanical tensile promotion of 110KBPSCCO superconductor. *Physica C: Superconductivity and Its Applications, 572*, Article 1353632.

[17] Sekkina, M. M. A., & Elsabawy, K. M. (2003). Mechanical tensile promotion and superconducting properties of highly Pb-content HTc-BPSCCO superconductor. *Materials Science and Engineering B, 103*(1), 71-76.

[18] Elsabawy, K. M., & Kandyel, E. E. (2007). Lead substitutions for promoted critical current density J_c and mechanical properties of $Mg_{1-x}Pb_xB_2$ regime. *Materials Research Bulletin, 42*(6), 1051–1060.

[19] Devamani, R. H. P., & Rani, M. J. (2014). Synthesis and characterization of lead chromate nanoparticles. *International Journal of Scientific Research, 3*(4), 398–402.

[20] Marchon, D., & Flatt, R. J. (2016). Mechanisms of cement hydration. In P.-C. Aïtcin & R. J. Flatt (Eds.), *Science and technology of concrete admixtures* (pp. 129–145). Elsevier.

[21] Chen, J., Jia, J., & Zhu, M. (2024). A critical review of the effect of chemical organic admixtures for OPC-based materials. *Materials Chemistry and Physics, 322*, Article 129591.

[22] Ye, P., Guo, B., Qin, H., Wang, C., Li, J., Chen, Y., Lu, D., Wang, L., Gao, P., Ma, P., Zhan, B., & Yu, Q. (2024). Investigation of the properties and sustainability of modified biochar-doped cement-based composite. *Cement and Concrete Composites, 153*, Article 105684.

[23] Roncero, J., Valls, S., & Gettu, R. (2002). Study of the influence of superplasticizers on the hydration of cement paste using nuclear magnetic resonance and X-ray diffraction techniques. *Cement and Concrete Research, 32*(1), 103–108.

[24] Mollah, M. Y. A., Palta, P., Hess, T. R., Vempati, R. K., & Cocke, D. L. (1995). Chemical and physical effects of sodium lignosulfonate superplasticizer on the hydration of Portland cement and solidification/stabilization consequences. *Cement and Concrete Research, 25*(3), 671–682.

[25] Mollah, M. Y. A., Lu, F., & Cocke, D. L. (1998). An X-ray diffraction (XRD) and Fourier transform infrared spectroscopic (FT-IR) characterization of the speciation of arsenic (V) in Portland cement type-V. *Science of the Total Environment, 224*(1–3), 57–68.

[26] Hanna, R. A., Barrie, P. J., Cheeseman, C. R., Hills, C. D., Buchler, P. M., & Perry, R. (1995). Solid state ^{29}Si and ^{27}Al NMR and FTIR study of cement pastes containing industrial wastes and organics. *Cement and Concrete Research, 25*(7), 1435–1444.

[27] Darweesh, H. H. M., Abdel-Kader, A. H., & El-Meligy, M. G. (2013). Utilization of pulp black liquor waste as a cement admixture. *International Journal of Basic and Applied Sciences, 2*(3), 230–238.

[28] Fayed, K., El-Hosiny, F. I., El-Kattan, I. M., Al-Kroom, H., Abd Elrahman, M., & Abdel-Gawwad, H. A. (2021). An innovative method for sustainable utilization of blast-furnace slag in the cleaner production of one-part hybrid cement mortar. *Materials, 14*(19), Article 5669.

[29] Elhabak, A., El-Sayed, H., El-Sokkary, T., Gharieb, M., & Abdel Aziz, A. (2023). The impact of local industrially produced metakaolin on both cement and concrete reinforcing steel physico-mechanical and corrosion resistance properties. *Egyptian Journal of Chemistry, 66*(10), 549–565.

[30] Akçaoğlu, T., Tokyay, M., & Çelik, T. (2004). Effect of coarse aggregate size and matrix quality on ITZ and failure behavior of concrete under uniaxial compression. *Cement and Concrete Composites, 26*(6), 633–638.

[31] Nemati, K. M., Monteiro, P. J. M., & Scrivener, K. L. (1998). Analysis of compressive stress-induced cracks in concrete. *ACI Materials Journal, 95*(5), 617–630.

[32] Portland Cement Association. (2002). *Types and Causes of Concrete Deterioration*. Portland Cement Association.

[33] Pourmortazavi, S. M., Hajimirsadeghi, S. S., & Nasrabadi, M. R. (2012). Applying the Taguchi robust design to optimization of the experimental conditions for synthesis of lead chromate nanorods. *Journal of Dispersion Science and Technology, 33*(2), 254–257.

[34] Ahmed, F. B., Ahsan, K. A., Shariff, T., & Meem, S. R. (2021). Formulation of polynomial equation predicting the splitting tensile strength of concrete. *Materials Today: Proceedings, 38*(5), 3269–3278.

[35] Qing, L., Shi, X., Mu, R., & Cheng, Y. (2018). Determining tensile strength of concrete based on experimental loads in fracture test. *Engineering Fracture Mechanics, 202*, 87–102.

[36] Hamed, N., El-Feky, M. S., Kohail, M., & Nasr, E.-S. A. R. (2019). Effect of nano-clay de-agglomeration on mechanical properties of concrete. *Construction and Building Materials, 205*, 245–256.

[37] Yehia, S. (2013). Effect of nano-clay on the mechanical properties of fresh and hardened cement mortar comparing with nano-silica. In *Proceedings of the Second International Conference on Materials, Energy and Environments (ICMEE)* (Yokohama, Japan, August 8–9, 2013).